MHD Mixed Convection Flow of Casson Nanofluid past a Stretching Sheet in the Presence of Viscous Dissipation, Chemical Reaction and Heat Source/Sink

K.Govardhan[1], G.Narender[2*] and G.Sreedhar Sarma[3]

[1] Department of Engineering Mathematics, GITAM University, Village Rudraram, Medak Dist.,Hyderabad-502329, Telangana State. INDIA. [2,3] Department of Humanities and Science, CVR College of Engineering, Mangalpalli, Ibrahimpatnam, R.R.Dist.,Hyderabad-501510, Telangana State, INDIA.

ABSTRACT

This paper focuses on the effect of MHD mixed convection flow of casson nanofluid past a stretching sheet in the presence of viscous dissipation, first order chemical reaction and heat source/sink. The profiles for the velocity, temperature and nanoparticle concentration depends on the parameters Casson fluid parameter β, concentration buoyancy parameter N, Hartman number M, radiation parameter R, Prandtl number Pr, the Schmidt number Sc, Brownian motion Nb, thermophoresis parameter Nt, Eckert number Ec, chemical reaction parameter γ the heat transfer Biot number γ_1 and the mass transfer Biot number γ_2. The constitute governing partial differential equation of flow, heat and mass transfer on considered flow are converted into nonlinear ordinary differential equations by employing suitable transformations and these transformed equations were solved by the Adam's Moultan fourth order method with shooting technique. The various numerical tables are calculated and tabulated. Our results have been compared with the results of a previous study and found to be in an excellent agreement.

Keywords: Nano Fluid, viscous dissipation, Brownian motion, Thermophoresis, Stretching Sheet, chemical reaction.

*Correspondence to Author:
G.Narender
Department of Humanities and Science, CVR College of Engineering, Mangalpalli, Ibrahimpatnam, R.R.Dist.,Hyderabad-501510, Telangana State, INDIA.

1. INTRODUCTION

The study of the boundary layer flow of an electrically conducting fluid through a porous media has many applications in manufacturing and natural process. The study includes the applications such as cooling of electronic devices by fans, cooling of nuclear reactors during emergency shutdown, cooling of an infinite metallic plate in a cooling bath, textile and paper industries, glass-fiber production, manufacture of plastic and rubber sheets, the utilization of geothermal energy, the boundary layer control in the field of aerodynamics, food processing, plasma studies and in the ow of biological fluids.

Magnetohydrodynamics(MHD) is the study of the flow of electrically conducting fluids in a magnetic field. Many theoretical and experimental studies on the conventional and electrically conducting fluids indicate that magnetic field markedly changes their heat transfer and transport characteristics. The study of magnetohydrodynamics has many important applications, and may be used to deal with problems such as cooling of nuclear reactors by liquid sodium and induction ow meter, which depends on the potential difference in the fluid in the direction perpendicular to the motion and to the magnetic field. Recently, the application of magnetohydrodynamics in the polymer industry and metallurgy has attracted the attention of many researchers. Several researches investigated the MHD flow.

Dissipation is the process of converting mechanical energy of downward-owing water into thermal and acoustical energy. Viscous dissipation is one of the interest for many applications: significant temperature rises are observed in polymer processing ows such as injection modeling or extrusion at high rates. Aerodynamic heating in the thin boundary layer around high speed aircraft raises the temperature of the skin. The flow due to stretching of a flat surface had been first investigated and reported by Crane [1]. Layek et al. [2] carried out heat and mass transfer analysis for boundary layer stagnation point flow of an incompressible viscous fluid towards a heated porous stretching sheet embedded in a porous medium subject to suction/blowing with internal heat generation or absorption. Hsiao [3] investigated a nanofluid flow with multimedia physical features for conjugate mixed convection and radiation.The study of non-Newtonian fluid flowing past stretching sheet was provided by Hartnett [4]. Aman and Ishak [5] studied the problem of mixed convection boundary layer flow adjacent to a stretching vertical sheet in an incompressible electrically conducting fluid. These are related studies to the present investigation about nanofluid flow. Turkyilmazoglu [6] studied about stretching/shrinking longitudinal fins of rectangular profile and heat transfer and related parameter effects. Makinde [7] discussed the transient free convection interaction with thermal radiation of an absorbing emitting fluid along moving vertical permeable plate. Recently Liu and Andersson [8] investigated heat transfer over a bidirectional stretching sheet with variable thermal conditions; it is mainly focused on the thermal energy conversion related problems at the couple boundary layer fluid flow system.

Mixed convective flows along with thermal radiations are commonly encountered in many environmental and scientific developments, for instance, in aeronautics, fire research, heating and cooling of channels, etc. Thus it is of great worth to study the radiative convective flow. Makinde [9] discussed the transient free convection interaction with thermal radiation of an absorbing emitting fluid along moving vertical permeable plate. Hayat et al. [10] explored the MHD radiative mixed convection boundary layer stagnation point flow through a porous medium. No doubt the MHD flow has gained considerable interest due to its fundamental importance in the industrial and technological applications such as in coating of metals, crystal growth, electromagnetic pumps, MHD generators and reactor cooling. The Lorentz force interacts with the buoyancy force in governing the flow and

temperature fields. The effect of Lorentz force is known to reduce the velocities. Heat and mass transfer characteristics in the magnetohydrodynamic (MHD) viscous flow over a permeable stretching surface is studied by Turkyilmazoglu [11]. Also, Motsa et al. [12] obtained the solutions for flow of upper-convected Maxwell fluid over porous stretching sheet in presence of the magnetic field by using successive Taylor series linearization method.

In several natural processes the fluids experience exothermic or endothermic chemical reactions. Hence it is important to discuss the effects of heat source or sink. Occurrence of heat source or sink may change the temperature distribution in the fluid which disturbs the particle deposition rate in systems such as nuclear reactors, electronic chips, and semiconductor wafers. Kandasamy et al. [13] discussed the combined effect of thermal diffusion and diffusion thermo in free convective heat and mass transfer flow over a porous stretching surface in the presence of hermophoresis particle deposition and heat source/sink. Recently, Hayat et al. [14] presented the radiative flow of Jeffery fluid in a porous medium with power law heat flux and heat source.

The present study deals with the convective boundary conditions in the mixed convection flow of nanofluid over a stretching sheet. Problem formulation is made in presence of thermal radiation, heat source/sink, viscous dissipation and first order chemical reaction. Casson fluid is taken as a base fluid. Boundary layer partial differential equations are reduced into set of ordinary differential equations by using appropriate transformations. Convergent solutions of the resulting problems are obtained by using series solution.Hayat et at.[15], homotopy analysis ethod Liu et al. [16], Hayat et al. [17], Abbasbandy et al. [18], Zheng et al. [19], Rashidi et al. [20]. Impacts of all embedding parameters are analyzed graphically for the temperature, concentration and flow fields. Numerical values of skin-friction coefficient, local

Nusselt and Sherwood numbers for different parameters are calculated and analyzed.

2. MATHEMATICAL MODELING

Consider two-dimensional steady-state MHD mixed convection flow of incompressible Casson nanofluid over a linear stretching surface with heat source/ sink. Flow is considered in the presence of an applied magnetic field, thermal radiation and first order chemical reaction. Convective heat and mass conditions are taken at surface of the sheet.The rheological equation of state for an isotropic and incompressible flow of a Casson fluid is

$$\tau_{ij} = \begin{cases} 2\left(\mu_{\mathrm{B}} + \frac{p_y}{\sqrt{2\pi}}\right)e_{ij}, \ \pi > \pi_c \\ 2\left(\mu_{\mathrm{B}} + \frac{p_y}{\sqrt{2\pi_c}}\right)e_{ij}, \ \pi_c > \pi \end{cases}$$

(1)

In the above expression where μ_{B} is the plastic dynamic viscosity of the non- Newtonian fluid, p_y is the yield stress of fluid, π is the product of the component of deformation rate and itself, namely, $\pi = e_{ij}e_{ij}$, e_{ij} is the (i,j) component of the deformation rate, and π_c is a critical value of π based on non-Newtonian model. The velocity field is taken as

$$V = [u(x,y), v(x,y), 0]$$

(2)

where u and v denote the velocity components in the x and y directions. The governing equations of mass, momentum, thermal energy, and concentration of steady, laminar boundary layer flow of a Casson nanofluid past a stretching sheet along with the boundary layer approximation are given by

$$\frac{\partial u}{\partial x} + \frac{\partial v}{\partial y} = 0 \qquad\qquad (3)$$

$$u\frac{\partial u}{\partial x} + v\frac{\partial u}{\partial y} = -\frac{\sigma^* B_0^2(x)}{\rho}u + \nu\left(1 + \frac{1}{\beta}\right)\frac{\partial^2 u}{\partial y^2} + g\beta_T(T - T_\infty) + g\beta_C(C - C_\infty) \qquad (4)$$

$$\frac{\partial T}{\partial x} + v\frac{\partial T}{\partial y} = \frac{\mu}{\rho c_p}\left(1 + \frac{1}{\gamma}\right)\left(\frac{\partial u}{\partial y}\right)^2 + \rho\frac{\partial^2 T}{\partial y^2} - \frac{16\sigma_s T_\infty^3}{3k_e \rho c_p}\frac{\partial^2 T}{\partial y^2} + \tau\left[D_B\frac{\partial C}{\partial y}\frac{\partial T}{\partial y} + \frac{D_T}{T_\infty}\left(\frac{\partial T}{\partial y}\right)^2\right] - \frac{Q}{\rho c_p}(T - T_\infty)$$

(5)

$$u\frac{\partial C}{\partial x} + v\frac{\partial C}{\partial y} = D_B \frac{\partial^2 C}{\partial y^2} + \frac{D_T}{T_\infty}\frac{\partial^2 C}{\partial y^2} - k_1(C - C_\infty) \quad (6)$$

where $\beta = \mu_B\sqrt{2\pi_c}/p_y$ is the Casson fluid parameter, β_T is the thermal expansion coefficient, β_C is the concentration expansion coefficient, $v = (\mu_B/\rho)$ is kinematic coefficient of viscosity, μ_B the dynamic viscosity, σ^* is electrical conductivity, ρ is density, T is temperature,C the concentration field, B_0 is magnitude of applied magnetic field, g the gravitational acceleration, $\tau = \frac{(\rho c)_p}{(\rho c)_f}$ is the ratio of effective heat capacity of the nanoparticle material and heat capacity of the fluid, D_B is Brownian diffusion coefficient, D_T is thermophoretic diffusion coefficient, c is specific heat at constant pressure σ_s the Stefan-Boltzmann constant, Q the uniform volumetric heat generation/absorption. The subscripts p and f stand for the thermophysical properties of nanoparticles and the base fluid, respectively.

The boundary conditions can be expressed as follow:

$$u = U_w(x) \Rightarrow u = cx, \qquad v = 0,$$

$$-k\frac{\partial T}{\partial y} = h(T_f - T), -D\frac{\partial C}{\partial y} = h^*(C_f - C) \text{ at } y = 0$$

$$u = 0, \ v = 0, \ T \rightarrow T_\infty, \ C \rightarrow C_\infty \text{ as } y = \infty \quad (7)$$

where subscript w corresponds to the wall condition, h the heat transfer coefficient, h^* the concentration transfer coefficient, T_f the hot fluid temperature and C_f the hot fluid concentration.

The continuity equation (1)can be satisfied by introducing a stream function ψ such that

$$u = \frac{\partial \psi}{\partial y}, \qquad v = -\frac{\partial \psi}{\partial x} \quad (8)$$

The momentum and energy equations can be transformed into the corresponding nonlinear ordinary differential equations by the following transformations:

$$\eta = y\sqrt{\frac{a}{v}}, \qquad \psi = \sqrt{avx}f(\eta),$$

$$\theta(\eta) = \frac{T - T_\infty}{T_f - T_\infty}, \qquad \phi(\eta) = \frac{C - C_\infty}{C_w - C_\infty}. \quad (9)$$

where ψ denotes stream function and $f(\eta)$ is a dimensionless velocity function, θ is dimensionless temperature function and ϕ is dimensionless concentration function and η is similarity variable. After using similarity transformations, the governing equations $(4) - (6)$ are reduced to the ordinary differential equations as follows:

$$\left(1 + \frac{1}{\beta}\right)f''' + ff'' - (f')^2 - Mf' + \lambda(\theta + N\phi) = 0 \quad (10)$$

$$\left(1 + \frac{4}{3}R\right)\theta'' + Prf\theta' + PrNb\theta'\phi' + PrNt(\theta')^2 + Pr\left(1 + \frac{1}{\gamma}\right)Ec\,(f'')^2 + Pr\beta_1\theta = 0 \quad (11)$$

$$\phi'' + Sef\phi' + \frac{Nt}{Nb}\theta'' - Sc\gamma\phi = 0 \quad (12)$$

The transformed boundary conditions for$f(\eta), \theta(\eta)$ and $\phi(\eta)$ are

$$f(0) = 0, \ f'(0) = 1, \ \theta'(0) = -\gamma_1[1 - \theta(0)], \phi' = -\gamma_2[1 - \phi(0)], \text{ at } \eta = 0,$$

$$f'(\infty) \rightarrow 0, \theta(\infty) \rightarrow 0, \phi(\infty) \rightarrow 0 \quad \text{as } \eta \rightarrow \infty \quad (13)$$

Here prime denotes differentiation with respect to η, λ is the mixed convection parameter, Gr_x the local Grashof number, N the concentration buoyancy parameter, Pr is Prandtl number, Se is Schmidt number, M is the Hartman number,R is the radiation parameter, Nb is Browian motation parameter,Nt is thermophoresis parameter, β_1 the heat source/sink parameter, γ_1 the heat transfer Biot number, γ_2 the mass transfer Biot number,Ec is the Eckert number and γ is the chemical reaction parameter. These can be defined in the forms

$$\lambda = \frac{Gr_x}{Re_x^2}, \qquad Sc = \frac{v}{D}, \qquad Nt = \frac{\rho_p D_B(C_w - C_\infty)}{\rho_f \alpha},$$

$$Gr_x = \frac{g\beta_T(T_f - T_\infty)x^3}{v^2}, \qquad M = \frac{\sigma^* B_0^2(x)}{\rho}, \qquad \beta_1 = \frac{Q}{\rho c_p},$$

$$N = \frac{\beta_C(C_w - C_\infty)}{\beta_T(T_w - T_\infty)}, \qquad R = \left(\frac{4\sigma^* T_\infty^3}{k_e k}\right), \qquad \gamma_1 = \frac{h}{k}\sqrt{\frac{v}{a}},$$

$$\Pr = \frac{\nu}{\alpha}, \qquad Nb = \frac{\rho_p D_B (C_w - C_\infty)}{\rho_f \alpha}, \qquad \gamma_2 = \frac{h^*}{D}\sqrt{\frac{\nu}{a}},$$

$$Ec = \frac{u^2}{c_p(T_f - T_\infty)}, \qquad \gamma = \frac{k_1}{c}.$$

The physical quantities of importance in stretching sheet transport are the skin friction coefficient C_f, the reduced Nusselt number Nu_x, and reduced Sherwood number Sh_x, which are calculated respectively by the following equations:

$$C_f = \frac{\tau_w}{\rho u_w^2}, Nu_x = \frac{x q_w}{k((T_w - T_\infty)}, Sh_x = \frac{x h_m}{D_B((C_w - C_\infty)}$$
(14)

where τ_w is the shear stress along the stretching surface, q_w is the heat flux from the stretching surface and h_w is the wall mass flux, which are given by

$$\tau_w = \mu\left(\frac{\partial u}{\partial y}\right)_{y=0}, q_w = -k\left(\frac{\partial T}{\partial y}\right)_{y=0},$$

$$h_m = -D_B\left(\frac{\partial C}{\partial y}\right)_{y=0} \qquad (15)$$

$$\frac{1}{2}C_f\sqrt{Re_x} = -\left(1 + \frac{1}{\beta}\right)f''(0), \quad \frac{Nu_x}{\sqrt{Re_x}} = -\theta'(0),$$

$$\frac{Sh_x}{\sqrt{Re_x}} = -\phi'(0)$$
(16)

where $R_{ex} = ax^2$ is the local Reynolds number.

3. NUMERICAL SOLUTION

Higher order nonlinear differential equations (10) – (12) are converted into a system of first order differential equations and further transformed into initial value problem by labeling the variables as

$$\begin{pmatrix} y_1' \\ y_2' \\ y_3' \\ y_4' \\ y_5' \\ y_6' \\ y_7' \end{pmatrix} = \begin{pmatrix} y_2 \\ y_3 \\ \frac{y_2^2 - y_1 y_3 - \lambda(y_4 + N y_6) + M y_2}{\left(1 + \frac{1}{\beta}\right)} \\ y_5 \\ \frac{-\Pr(y_1 y_5 + Nb y_7 y_5 + Nt y_5^2 + \beta_1 y_4)}{\left(1 + \frac{4R}{3}\right)} \\ y_7 \\ -Sc y_7 y_1 - \frac{Nb}{Nt} y_5^1 + sc\gamma y_6 \end{pmatrix}$$
(17)

Associated boundary conditions in Eq. (13) can be written as

$$\begin{pmatrix} y_1(0) \\ y_2(0) \\ y_3(0) \\ y_4(0) \\ y_5(0) \\ y_6(0) \\ y_7(0) \end{pmatrix} = \begin{pmatrix} 0 \\ 1 \\ p_1 \\ p_2 \\ \gamma_1(p_2 - 1) \\ p_3 \\ \gamma_2(p_3 - 1) \end{pmatrix} \qquad (18)$$

Here $p_1 = f''(0), p_2 = \theta(0) and\ p_3(0) = \phi(0)$.

p_1, p_2, p_3 are to be found satisfying end conditions $y_2 \to 0, y_4 \to 0, y_6 \to 0$ as $\eta \to \infty$. Adams Moultan fourth order method (with the corresponding predictor) is used to solve the initial value problem. Assumed values of p_1, p_2 and p_3 are corrected using Newton method.

Derivatives of $f''(\infty, p_1, p_2, p_3)$, $\theta(\infty, p_1, p_2, p_3)$ and $\phi(\infty, p_1, p_2, p_3)$ with respect to any parameter $p(p_1, p_2\ or\ p_3)$ are found by solving the equation which are obtained by differentiating system (17).

$$Y_i = \frac{\partial y_i}{\partial p} \text{ for all } i = 1,2,3,4,5,6,7$$

These equations are

$$Y_1' = Y(2), Y_2' = Y(3),$$

$$Y_3' = 2y(2)Y(2) - y(1)Y(3) - Y(1)y(3) - \lambda(y(4) + Ny(6)) + My(2),$$

$$Y_4' = Y(5),$$

$$Y_5' = \frac{-\Pr}{\left(1 + \frac{4}{3}\right)}[y(1)Y(5) - Y(1)y(5) + Nb(y(7)Y(5) - Y(7)y(5) + 2Nty(5)Y(5) + \beta_1 y(4)],$$

$$Y_6' = Y(7),$$

$$Y_7' = -Sc(Y(7)y(1) + Y(1)y(7)) - \frac{Nt}{Nb}Y_5' + Sc\gamma y(6)$$

This system is solved with three different sets of initial conditions $y_i(0) = 0$ for all $i = 1,2,3,4,5,6,7$ expect

(i) $y_3(0) = 1,$

(ii) $y_4(0) = 1, y_5(0) = \gamma_1,$

(iii) $y_6(0) = 1, y_7(0) = \gamma_2.$

Newton's method is

$$\begin{pmatrix} p_1 \\ p_2 \\ p_3 \end{pmatrix}^{New} = \begin{pmatrix} p_1 \\ p_2 \\ p_3 \end{pmatrix}^{Old}$$

$$- \begin{bmatrix} \dfrac{\partial y_3}{\partial p_1} & \dfrac{\partial y_3}{\partial p_2} & \dfrac{\partial y_3}{\partial p_3} \\[2mm] \dfrac{\partial y_4}{\partial p_1} & \dfrac{\partial y_4}{\partial p_2} & \dfrac{\partial y_4}{\partial p_3} \\[2mm] \dfrac{\partial y_6}{\partial p_1} & \dfrac{\partial y_6}{\partial p_2} & \dfrac{\partial y_6}{\partial p_3} \end{bmatrix}_{\eta=\infty}^{-1} \begin{bmatrix} y_3 \\ y_4 \\ y_6 \end{bmatrix}_{\eta=\infty}$$

(19)

It may be noticed that the choice of initial guess of p_1, p_2, p_3 is very crucial. Once we obtain solution for a particular set of physical parameters, a single parameter changed slightly to achieve convergence of newton's method. The choice of $\eta_{max} = 8$ was more than enough for end condition. The convergence criteria is chosen to be successive value agree up to 3 significant digits.

4. RESULTS AND DISCUSSION

In the present study, the effects MHD Mixed convection flow of Casson Nanofluid past a stretching sheet in the presence of viscous dissipation, chemical reaction and heat source/sink were analyzed. In order to analyze the results, numerical calculations are carried out for various values of Casson fluid parameter β, concentration buoyancy parameter N, the mixed convection parameter λ, Brownian motion Nb, thermophoresis parameter Nt, Eckert number Ec, chemical reaction parameter γ the heat transfer Biot number γ_1 and the mass transfer Biot number γ_2. For validation of the present method, the results are compared with previously reported results and displayed in Tables 1, 2, and 3. Results are presented in several tables so that variation with respect to a single parameter can be studied.

Table 1 represents the variation of both local nusselt number $-\theta(0)$ and Sherwood number $-\phi(0)$ for different values of the parameters β, Nt and Nb. As the values of Casson fluid parameter β and thermophoresis parameter Nt increase, both the values of $-\theta(0)$ and $-\phi(0)$ decrease.

Tables 2 prepared to explore the impacts of mixed convection parameter λ, concentration buoyancy parameter N, heat transfer Biot number γ_1 and mass transfer Biot number γ_2 on local Nusselt and Sherwood numbers. In case of assisting flow ($\lambda > 0$) and with an enhancement in N, γ_1, γ_2 the local Nusselt and Sherwood numbers enhance. **Table 3** describes the comparison of skin-friction coefficient for different values of $\beta, Nt, Nb, \gamma_1, \gamma_2, \lambda, N$ respectively.

TABLE 1 Comparison of Numerical values of Local Nusselt Number $-\theta'(0)$ and Sherwood Number $-\phi'(0)$ for different values of parameters β, Nt, Nb When $\beta_1 = R = M = \gamma = 0.0, \lambda = N = 0.3, \gamma_1 = \gamma_2 = 0.2, Pr = 1.0, Sc = 0.7$.

β	Nt	Nb	$-\theta'(0)$		$-\phi'(0)$	
			T.Hayat et al.[01]	Present Result	T.Hayat et al.[01]	Present Result
0.5	0.2	0.2	0.15271	0.1526939	0.12054	0.1205407
0.7			0.15204	0.1519901	0.11910	0.1188185
0.9			0.15150	0.1514782	0.11758	0.1175741
0.5	0.4		0.15195	0.1518633	0.096142	0.0956810
	0.6		0.15106	0.1510139	0.071520	0.0717563
		0.4	0.15186	0.1517981	0.13368	0.1336129
		0.6	0.15100	0.1509065	0.13815	0.1379848

TABLE 2 Comparison of Numerical Values of Local Nusselt Number $-\theta'(0)$ And Sherwood Number $-\phi'(0)$ for Different values of Parameters $\lambda, N, \gamma_1, \gamma_2$ when $\beta_1 = R = M = \gamma = Ec = 0.0, Nt = Nb = 0.2, \beta = 0.5, Pr = 1.0, Sc = 0.7$.

λ	N	γ_1	γ_2	$-\theta'(0)$		$-\phi'(0)$	
				T.Hayat et al.[01]	Present Result	T.Hayat et al.[01]	Present Result
-0.5	0.3	0.2	0.2	1.5201	0.1411910	0.11969	0.0840725
0.0				0.15248	0.1524246	0.12014	0.1199470
0.3				0.15271	0.1526939	0.12054	0.1205407
0.6				0.15302	0.1529436	0.12144	0.1210837
0.3	0.0			0.15261	0.1525648	0.12032	0.1202398
	0.3			0.15271	0.1526939	0.12054	0.1205407
	0.6			0.15302	0.1528177	0.12078	0.1208268
0.3	0.3	0.2		0.15271	0.1526939	0.12054	0.1205407
		0.4		0.24602	0.2458604	0.10535	0.1053597
		0.6		0.30822	0.3080297	0.095273	0.0954224
0.3	0.3	0.2	0.1	0.15304	0.1529687	0.069638	0.0694951
			0.3	0.15255	0.1524822	0.15995	0.0694951
			0.5	0.15224	0.1521774	0.21584	0.2156148

TABLE 3 Comparison Numerical values of skin-friction coefficient $-\left(1+\frac{1}{\beta}\right)f''(0)$ for different values of parameters $\beta, Nt, Nb, \lambda, N, \gamma_1, \gamma_2$ when $\beta_1 = R = M = Ec = \gamma = 0.0, Pr = 1.0, Sc = 0.7$.

β	Nt	Nb	λ	N	γ_1	γ_2	$-\left(1+\frac{1}{\beta}\right)f''(0)$	
							T.Hayat et al.[01]	Present Result
0.5	0.2	0.2	0.3	0.3	0.2	0.2	1.6532	1.6550370
0.7							1.4797	1.4804710
0.9							1.3741	1.3746860
0.5	0.4						1.6368	1.6384980
	0.6						1.6204	1.6222260
0.5	0.2	0.4					1.6598	1.6615690
		0.6					1.6613	1.6629120
0.5	0.2	0.2	-0.5	0.3	0.2	0.2	1.8689	1.8719940
			0.0				1.7321	1.7340090
			0.3				1.6532	1.6550370
			0.6				1.5770	1.5784280
			0.3	0.0			1.6863	1.6881400
				0.3			1.6532	1.6550370
				0.6			1.6207	1.6225270
0.5	0.2	0.2	0.3	0.3	0.2		1.6532	1.6550370
					0.4		1.6152	1.6169630
					0.6		1.5893	1.5912010
0.5	0.2	0.2	0.3	0.3	0.2	0.1	1.6598	1.6614870
						0.3	1.6484	1.6501050
						0.5	1.6413	1.6430600

TABLE 4 Computation showing the values of skin-friction coefficient $-\left(1+\frac{1}{\beta}\right)f''(0)$, of Local Nusselt Number $-\theta'(0)$ and Sherwood Number $-\phi'(0)$ for different values of parameters λ, Ec when $\beta_1 = R = M = \gamma = 0.0, Nt = Nb = \gamma_1 = \gamma_2 = 0.2, \beta = N = 0.5, Pr = 1.0, Sc = 0.7$.

λ	$Ec = 0$			$Ec = 0.2$			$Ec = 0.5$		
	$-\left(1+\frac{1}{\beta}\right)f''(0)$	$-\theta'(0)$	$-\phi'(0)$	$-\left(1+\frac{1}{\beta}\right)f''(0)$	$-\theta'(0)$	$-\phi'(0)$	$-\left(1+\frac{1}{\beta}\right)f''(0)$	$-\theta'(0)$	$-\phi'(0)$
-0.5	1.9134680	0.1517340	0.1183575	2.0048810	0.1145943	0.1333708	2.2170020	0.0369943	0.1622329
-0.3	1.8396380	0.1520290	0.1190451	1.8874780	0.1184620	0.1331941	1.9710430	0.0611734	0.1570865
-0.1	1.7686150	0.1522982	0.1196611	1.7828940	0.1215222	0.1330002	1.8052610	0.0736003	0.1537356
0	1.7340080	0.5780027	0.4002650	1.7340090	0.1228466	0.1329055	1.7340090	0.0783029	0.1523838
0.1	1.6999460	0.1525462	0.1202202	1.6869410	0.1240642	0.1328142	1.6678620	0.0823799	0.1511822
0.3	1.6332990	0.1527770	0.1207329	1.5973510	0.1262383	0.1326443	1.5469270	0.0891988	0.1491229
0.5	1.5684230	0.1529929	0.1212069	1.5127120	0.1281345	0.1324927	1.4371370	0.0947593	0.1474091

TABLE 5 Computation showing the values of skin-friction coefficient $-\left(1+\frac{1}{\beta}\right)f''(0)$, of Local Nusselt Number $-\theta'(0)$ and Sherwood Number $-\phi'(0)$ for different values of parameters β, Ec when $\beta_1 = R = M = \gamma = 0.0, \lambda = 0.3, Nt = Nb = \gamma_1 = \gamma_2 = 0.2, N = 0.5, Pr = 1.0, Sc = 0.7$.

β	$Ec = 0$			$Ec = 0.2$			$Ec = 0.5$		
	$-\left(1+\frac{1}{\beta}\right)f''(0)$	$-\theta'(0)$	$-\phi'(0)$	$-\left(1+\frac{1}{\beta}\right)f''(0)$	$-\theta'(0)$	$-\phi'(0)$	$-\left(1+\frac{1}{\beta}\right)f''(0)$	$-\theta'(0)$	$-\phi'(0)$
0.5	1.6332990	0.1527770	0.1207329	1.5973510	0.1262383	0.1326443	1.5469270	0.0891988	0.1491229
0.7	1.4588750	0.1521000	0.1190783	1.4274150	0.1274774	0.1302837	1.3835310	0.0931757	0.1457792
0.9	1.3532000	0.1516110	0.1178925	1.3244610	0.1282154	0.1286471	1.2845170	0.0956635	0.1435128

TABLE 6 Computation showing the values of skin-friction coefficient $-\left(1+\frac{1}{\beta}\right)f''(0)$, of Local Nusselt Number $-\theta'(0)$ and Sherwood Number $-\phi'(0)$ for different values of parameters Nt, Ec when $\beta_1 = R = M = \gamma = 0.0, \lambda = 0.3, Nb = \gamma_1 = \gamma_2 = 0.2, \beta = N = 0.5, Pr = 1.0, Sc = 0.7$.

Nt	$Ec = 0$			$Ec = 0.2$			$Ec = 0.5$		
	$-\left(1+\frac{1}{\beta}\right)f''(0)$	$-\theta'(0)$	$-\phi'(0)$	$-\left(1+\frac{1}{\beta}\right)f''(0)$	$-\theta'(0)$	$-\phi'(0)$	$-\left(1+\frac{1}{\beta}\right)f''(0)$	$-\theta'(0)$	$-\phi'(0)$
0.2	1.6332990	0.1527770	0.1207329	1.5973510	0.1262383	0.1326443	1.5469270	0.0891988	0.1491229
0.4	1.6070970	0.1519914	0.0961043	1.5741970	0.1258140	0.1193705	1.5283700	0.0893571	0.1515359
0.6	1.5815300	0.1511874	0.0724873	1.5517590	0.1253514	0.1067416	1.5106090	0.0894192	0.1540931

TABLE 7 Computation showing the values of skin-friction coefficient $-\left(1+\frac{1}{\beta}\right)f''(0)$, of Local Nusselt Number $-\theta'(0)$ and Sherwood Number $-\phi'(0)$ for different values of parameters Nb, Ec when $\beta_1 = R = M = \gamma = 0.0, \lambda = 0.3, Nt = \gamma_1 = \gamma_2 = 0.2, \beta = N = 0.5, Pr = 1.0, Sc = 0.7$.

Nb	$Ec = 0$			$Ec = 0.2$			$Ec = 0.5$		
	$-\left(1+\frac{1}{\beta}\right)f''(0)$	$-\theta'(0)$	$-\phi'(0)$	$-\left(1+\frac{1}{\beta}\right)f''(0)$	$-\theta'(0)$	$-\phi'(0)$	$-\left(1+\frac{1}{\beta}\right)f''(0)$	$-\theta'(0)$	$-\phi'(0)$
0.2	1.6332990	0.1527770	0.1207329	1.5973510	0.1262383	0.1326443	1.5469270	0.0891988	0.1491229
0.4	1.6448500	0.1518615	0.1337213	1.6066600	0.1247386	0.1398785	1.5529160	0.0868544	0.1483897
0.6	1.6478890	0.1509639	.1380702	1.6086540	0.1234832	0.1422799	1.5534280	0.0851180	0.1480930

TABLE 8 Computation showing the values of skin-friction coefficient $-\left(1+\frac{1}{\beta}\right)f''(0)$, of Local Nusselt Number $-\theta'(0)$ and Sherwood Number $-\phi'(0)$ for different values of parameters γ_1, Ec when $\beta_1 = R = M = \gamma = 0.0, \lambda = 0.3, Nt = Nb = \gamma_2 = 0.2, \beta = N = 0.5, Pr = 1.0, Sc = 0.7$.

γ_1	$Ec = 0$			$Ec = 0.2$			$Ec = 0.5$		
	$-\left(1+\frac{1}{\beta}\right)f''(0)$	$-\theta'(0)$	$-\phi'(0)$	$-\left(1+\frac{1}{\beta}\right)f''(0)$	$-\theta'(0)$	$-\phi'(0)$	$-\left(1+\frac{1}{\beta}\right)f''(0)$	$-\theta'(0)$	$-\phi'(0)$
0.2	1.6332990	0.1527770	0.1207329	1.5973510	0.1262383	0.1326443	1.5469270	0.0891988	0.1491229
0.4	1.5894870	0.2461417	0.1056592	1.5618180	0.2043547	0.1198786	1.5224360	0.1453078	0.1398094
0.6	1.5599890	0.3085376	0.0957952	1.5376830	0.2570481	0.1114108	1.5056090	0.1836398	0.1335182

TABLE 9 Computation showing the values of skin-friction coefficient $-\left(1+\frac{1}{\beta}\right)f''(0)$, of Local Nusselt Number $-\theta'(0)$ and Sherwood Number $-\phi'(0)$ for different values of parameters γ_2, Ec when $\beta_1 = R = M = \gamma = 0.0, \lambda = 0.3, Nt = Nb = \gamma_1 = 0.2, \beta = N = 0.5, Pr = 1.0, Sc = 0.7$.

γ_2	$Ec = 0$			$Ec = 0.2$			$Ec = 0.5$		
	$-\left(1+\frac{1}{\beta}\right)f''(0)$	$-\theta'(0)$	$-\phi'(0)$	$-\left(1+\frac{1}{\beta}\right)f''(0)$	$-\theta'(0)$	$-\phi'(0)$	$-\left(1+\frac{1}{\beta}\right)f''(0)$	$-\theta'(0)$	$-\phi'(0)$
0.1	1.6436920	0.1530387	0.0695723	1.6085930	0.1264281	0.0764359	1.5593180	0.0892665	0.0859309
0.3	1.6253620	0.1525752	0.1599624	1.5887610	0.1260910	0.1757466	1.5374660	0.0891444	0.1975839
0.5	1.6140230	0.1522842	0.2162008	1.5764960	0.1258770	0.2375431	1.5239520	0.0890614	0.2670726

Figures 1–4 are drawn to explore the behavior of Casson fluid parameter β, Hartman number M, mixed convection parameter λ and concentration buoyancy parameter N on velocity profile $f'(\eta)$. Fig. 1 reveals that the velocity profile $f'(\eta)$ and momentum boundary layer thickness decrease with an increase in Casson parameter β. Effect of Hartman number M on the velocity profile $f'(\eta)$ is displayed in Fig. 2. With an increase in M the velocity profile $f'(\eta)$ decreases. Also, momentum boundary layer thicknesses is a decreasing functions of M. This is due to the reason that with an increase in M the Lorentz force increases which resist the flow. Fig. 3 is plotted to analyze the influence of mixed convection parameter λ on the velocity profile $f'(\eta)$ in both assisting and opposing flows. It is observed that the velocity profile $f'(\eta)$ and momentum boundary layer thickness increase when $\lambda > 0$ (assisting flow) while opposite behavior is noted for $\lambda <$ (opposing flow). It is examined that the momentum boundary layer thickness and velocity profile $f'(\eta)$ increase with an increase in N (see Fig. 4).

The effect of Brownian motion parameter Nb on temperature $\theta(\eta)$ and concentration $\phi(\eta)$ are presented in Fig. 5 and 6. The Fig. 5 represents the variation of the dimensionless temperature with the Brownian motion parameter Nb. Increase in Nb values gives the temperature graph increase and increase in thermal boundary layer thickness. As increase in Nb, due to movement of nanoparticles, results in increase the kinetic energy of the nanoparticle, thus rises the temperature for both constant surface temperature and prescribed surface temperature. It is also noticed that the concentration $\phi(\eta)$ and associated boundary layer thickness reduces with an enhancement in Nb.

Fig. 7 is designated to see the effect of Prandtl number Pr on temperature profiles. Physically, the Prandtl number is inversely proportional to the thermal diffusivity. Hence, larger values of Pr produce weaker thermal diffusivity. This corresponds to a reduction in both temperature and the associated boundary layer thickness.

Fig. 8 is sketched for a better understanding of the impact of Sc on concentration profiles $\phi(\eta)$. Physically, Schmidt number is inversely proportional to the mass diffusion, therefore an increase in Sc causes a reduction in nanoparticle concentration profiles, as well as in related boundary layer thickness.

Fig. 9 is plotted to interpret the impact of heat generation parameter on temperature profile. This figure illustrates that the temperature field increases with the increase in heat generation parameter. This fact is physically true because by increasing values of β_1 i.e. $\beta_1 > 0$, exothermic reactions occurred in the system and as a consequence large amount of heat is evolved which raises the temperature of fluid distribution.

Fig. 10 describes the influence of β_1 on $\phi(\eta)$. It is exposed that $\phi(\eta)$ decays near the stretching surface however it enhances as one moves away from the surface. The thickness of concentration boundary layer also enhances by increasing the value of β_1.

Fig. 11 reveals the changes that are noticed in nanofluid temperature profiles due to increase in the values of thermal radiation parameter R. It is worth noticing that the nanofluid temperature increases as thermal radiation increase due to the fact that the conduction impact of the nanofluid improves in the presence of thermal radiation. Hence higher values of radiation parameter mean higher surface heat flux and so, enhance the temperature within the boundary layer region.

It is concluded from Fig. 12 and 13, that the increase in thermopheretic parameter Nt increases the nanofluid temperature. The increase in the temperature is viewed as a result of the thermophoresis force by which a nanoparticle pushes the other nanoparticles away from the heated surface which in turn generates thermal energy due to the collision of nanoparticles. On the other hand, the effect of thermopheretic force on nanoparticle

concentration is only significant in a region away from the surface where it increases with the increase in thermopheretic force. It is clearly observed that the nanofluid temperature increases with the increase in convective heating of the surface. Also there is an increase in the nanoparticle concentration with the increase in convective heating of the surface.

Fig. 15 is plotted to explore the impact of γ_1 on $\theta(\eta)$. Physically, the Biot number is the ratio of internal thermal resistance at the surface of the body to the boundary layer thermal resistance. Therefore, enhancing the values of γ_1 shows an increase in temperature profiles and its related boundary layer thickness. We see in Fig. 16 it was observed that as the convective heating of the sheet is enhanced i.e. γ_1 increases, the thermal penetration depth increases. Because the concentration distribution is driven by the temperature field, one anticipates that a higher Biot number γ_1 would promote a deeper penetration of the concentration.

Fig. 17 shows the effect of chemical reaction parameter γ on concentration profile. Chemical reaction parameter reduces the concentration profile. This is true because as chemical reaction takes place, the amount of nanoparticles within the fluid is getting smaller and smaller. According to the definition of Eckert number Ec, a positive Ec corresponds to fluid heating (heat is being supplied across the wall into the fluid) case $(T_w - T_\infty)$ so that the fluid is being heated whereas a negative Ec means that the fluid is being cooled. From Fig. 18 it is seen that the dimensionless temperature increases when the fluid is being heated($Ec > 0$). It is noticed from Fig.18 that concentration profiles first decrease near the sheet surface where $0 \leq \eta \leq 2$ and situation is completely reversed in the other part of the boundary layer flow where $\eta \geq 2$.
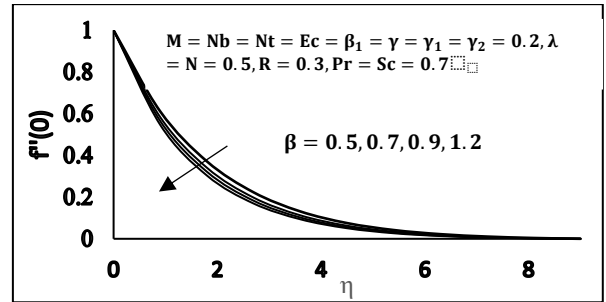
Fig. 1. Variation of β on $f(\eta)$.
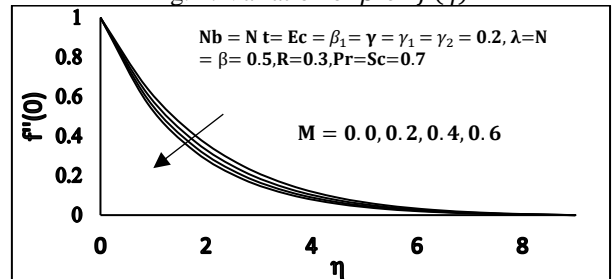
Fig. 2. Variation of M on $f(\eta)$.
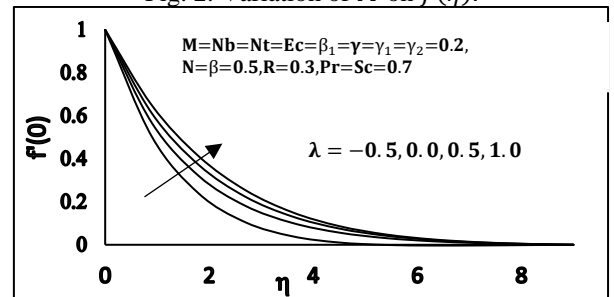
Fig. 3. Variation of λ on $f(\eta)$.
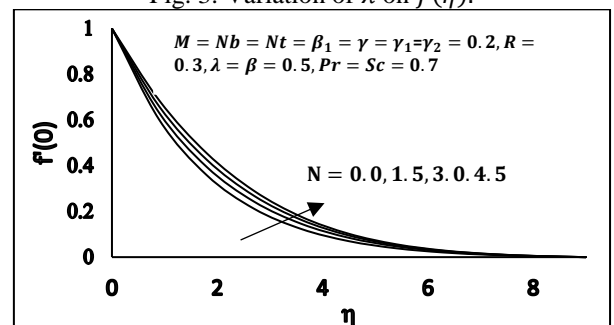

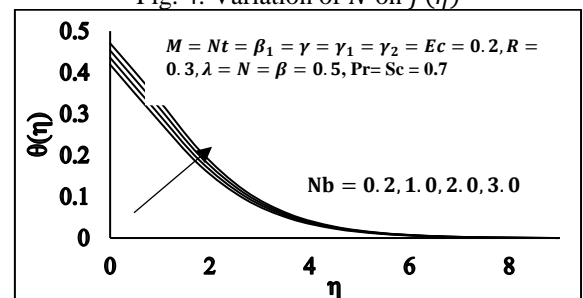Fig. 4. Variation of N on $f(\eta)$
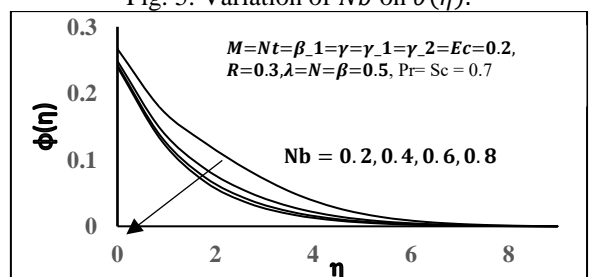

Fig. 5. Variation of Nb on $\theta(\eta)$.

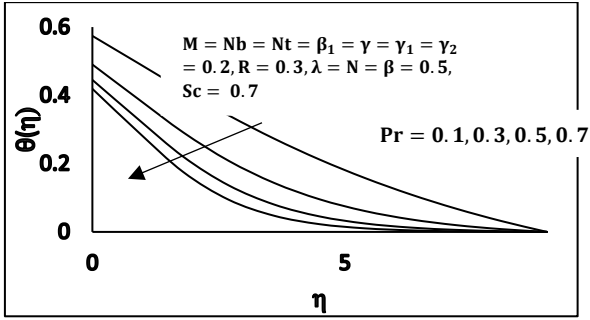Fig. 6. Variation of Nb on $\phi(\eta)$.

Fig. 7. Variation of Pr on $\theta(\eta)$.

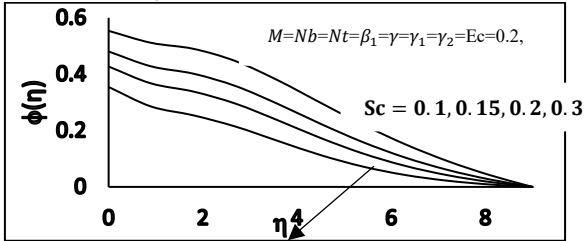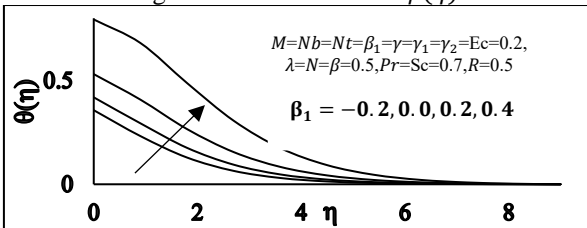Fig. 8.Variation of Sc on $\phi(\eta)$.

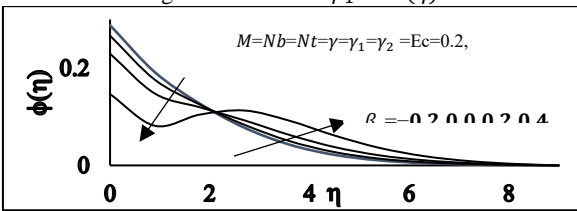Fig. 9. Variation of β_1 on $\theta(\eta)$.

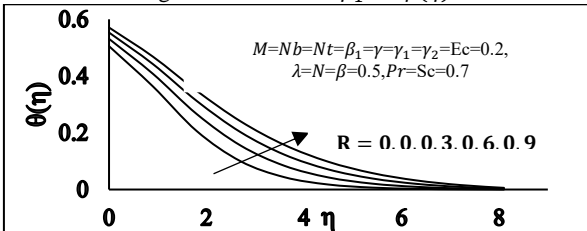
Fig. 10. Variation of β_1 on $\phi(\eta)$.

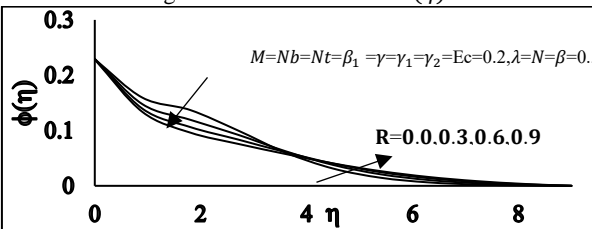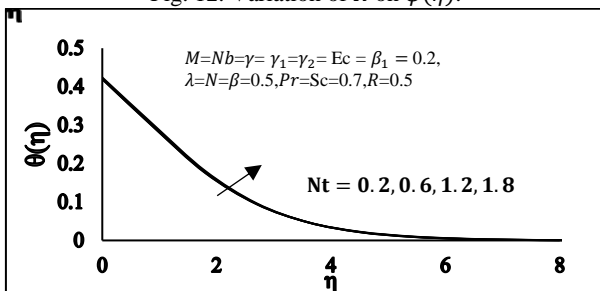Fig. 11. Variation of R on $\theta(\eta)$.

Fig. 12. Variation of R on $\phi(\eta)$.
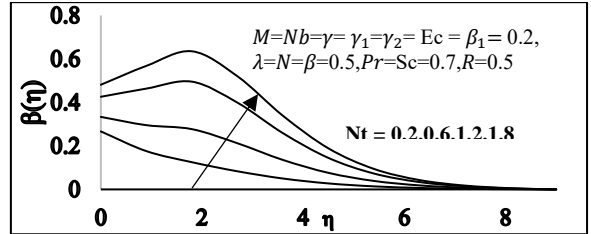

Fig. 13. Variation of Nt on $\theta(\eta)$.
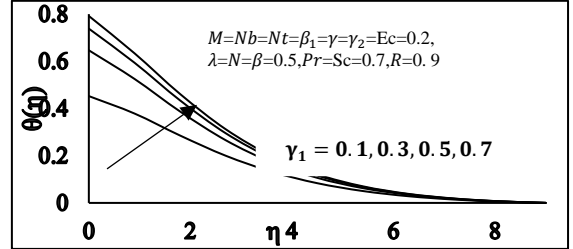

Fig. 14. Variation of Nt on $\phi(\eta)$.
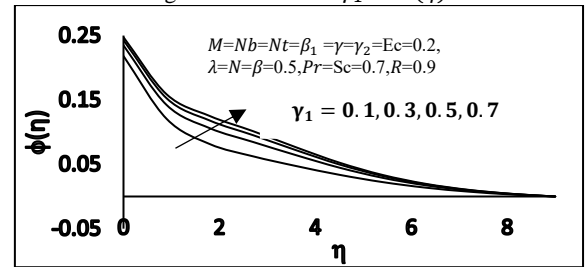

Fig. 15.Variation of γ_1 on $\theta(\eta)$.
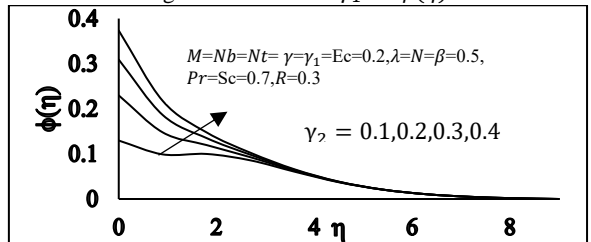

Fig. 16.Variation of γ_1 on $\phi(\eta)$.

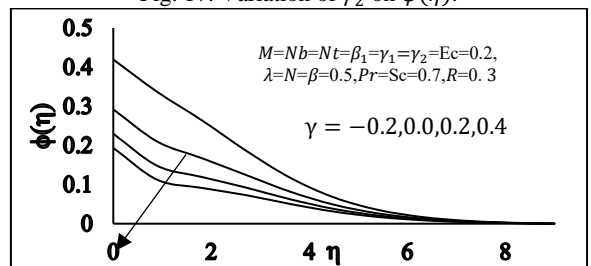Fig. 17. Variation of γ_2 on $\phi(\eta)$.

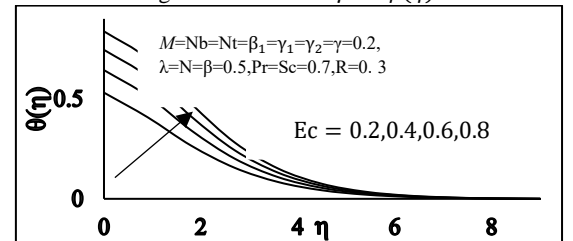Fig. 18 Variation of γ on $\phi(\eta)$.
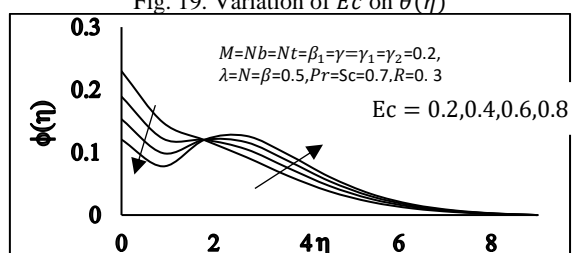

Fig. 19. Variation of Ec on $\theta(\eta)$

Fig. 20. Variation of Ec on $\phi(\eta)$

5. CONCLUSION

In the present work effect of MHD Mixed convection Flow of Casson Nanofluid past a stretching sheet in the presence of viscous dissipation, first order chemical reaction and heat source/sink is investigated. We come to the following conclusions,

a) The velocity profile $f'(\eta)$ and thickness of velocity boundary layer decreases with an increase in casson parameter β and magnetic field parameter M.

b) The temperature boundary layer thickness increases due to increase of Radiation parameter whereas concentration boundary layer thickness decreases due to increase of Radiation parameter.

c) The temperature boundary layer thickness increases due to increase of Eckert number where as concentration boundary layer thickness decreases due to increase of Eckert number. Also the surface heat transfer rate is increased.

d) The temperature boundary layer thickness increases due to increase of Brownian motion parameter. Also the heat transfer rate at the sheet increases for increasing value of Brownian motion parameter and Thermophoresis parameter. The concentration boundary layer thickness increases due to increase of Thermophoresis parameter and concentration boundary layer thickness decreases due to increase of Brownian motion parameter. Also the mass transfer rate at the sheet decreases due to decrease of Brownian motion parameter.

e) Heat source increases the temperature while as reverse occurred with a heat sink.

f) The dimensionless temperature and nanoparticle concentration profiles increase with increase in γ_1 and γ_2 respectively.

REFERENCES

[1] Crane LJ. Flow past a stretching plate. Z Angew Math Phys (1970); 21(4):645–7.

[2] Layek GC, Mukhopadhyay S, Samad SK. Heat and mass transfer analysis for boundary layer stagnation point flow towards a heated porous stretching sheet with heat absorption/generation and suction/blowing. Int. Commun Heat Mass Transfer (2007); 34:347–56.

[3] K.-L. Hsiao, Nanofluid flow with multimedia physical features for conjugate mixed convection and radiation, Comput. Fluids 104 (2014) 1–8.

[4] J.P. Hartnett, Viscoelastic fluids: a new challenge in heat transfer, Trans. ASME (1992) 296–303.

[5] F. Aman, A. Ishak, Hydromagnetic flow and heat transfer adjacent to a stretching vertical sheet with prescribed surface heat flux, Heat Mass Transf. 46 (6) (2009) 615–620.

[6] M. Turkyilmazoglu, Stretching/shrinking longitudinal fins of rectangular profile and heat transfer, Energy Convers. Manag. 91 (2015) 199–203.

[7] Makinde, O. D., Free convection flow with thermal radiation and mass transfer past a moving vertical porous plate. International *Communications in Heat and Mass Transfer (*2005*)*; 32(10), 1411-1419.

[8] Hayat, T., Z. Abbas, I. Pop and S. Asghar, Effects of radiation and magnetic field on the mixed convection stagnation-point flow over a vertical stretching sheet in a porous medium. *International Journal of Heat and MassTransfer* (2010); 53(1-3), 466-474.

[9] I.-C. Liu, H.I. Andersson, Heat transfer over a bidirectional stretching sheet with variable thermal conditions, Int. J. Heat Mass Transf. 51 (15–46) (2008) 4018–4024.

[10] Makinde, O. D., Free convection flow with thermal radiation and mass transfer past a moving vertical porous plate. International *Communications in Heat and Mass Transfer* (2005); 32(10), 1411-1419.

[11] Hayat, T., Z. Abbas, I. Pop and S. Asghar, Effects of radiation and magnetic field on the mixed convection stagnation-point flow over a vertical stretching sheet in a porous medium. *International Journal of Heat and Mass Transfer* (2010); 53(1-3), 466-474.

[12] Turkyilmazoglu, M., Analytic heat and mass transfer of the mixed hydrodynamic/thermal slip MHD viscous flow over a stretching sheet. *International Journal Of Mechanical Sciences* (2011); 53(10), 886-896.

[13] Motsa, S. S., T. Hayat and O. M. Aldossary , MHD flow of upper- convected Maxwell fluid over porous stretching sheet using successive Taylor series linearization method. *Applied Mathematics and Mechanics* (2012); 33(8), 975-990.

[14] Kandasamy, R., T. Hayat and S. Obadiah., Group theory transformation for Soret and Dufour effects on free convective heat and mass transfer with thermophoresis and chemical reaction over a porous stretching surface in the presence of heat source/sink. Nuclear Engineering and Design (2011); 241, 2155 – 2161.

[15] Hayat, T., S. A. Shehzad, M. Qasim and S. Obaidat , Radiative flow of Jeffery fluid in a porous medium with power law heat flux and heat source. *Nuclear Engineering and Design* (2012); 243, 15-19.

[16] T Hayat et al, Mixed Convection Flow of Casson Nanofluid over a Stretching Sheet with Convectively Heated Chemical Reaction and Heat Source/Sink, *Journal of Applied Fluid Mechanics*, (2015); Vol. 8, No. 4, pp. 803-813.

[17] Liu, Y.P., S. J. Liao and Z. B. Li, Symbolic computation of strongly nonlinear periodic oscillations. *Journal of Symbolic Computa tion* (2013); 55, 72-95.

[18] Hayat, T., S. A. Shehzad, M. B. Ashraf and A. Alsaedi, Magnetohydrodynamic mixed convection flow of thixotropic fluid with thermophoresis and Joule heating. *Journal of Thermophysics and Heat Transfer* (2013); 27, 733-740.

[19] Abbasbandy, S., M. S. Hashemi and I. Hashim, On convergence of homotopy analysis method and its application to fractional integro-differential equations. *Quaestiones Mathematicae* (2013); 36(1), 93-105.

[20] Zheng, L., J. Niu, X. Zhang and Y. Gao (2012). MHD flow and heat transfer over a porous shrinking surface with velocity slip and temperature jump. *Mathematical and Computer Modelling* 56(5-6), 133-144.

[21] Rashidi, M. M., N. Kavyani and S. Abelman, Investigation of entropy generation in MHD and slip flow over a rotating porous disk with variable properties. *International Journal of Heat and Mass Transfer* (2014); 70, 892-917.

NOMENCLATURE

c	constant associated with linear stretch
B_0	applied magnetic field
Bi	Biot number
C	nanoparticle volume fraction
C_f	skin-friction coefficient
C_p	specific heat at constant pressure
C_w	wall nanoparticle volume fraction
C_∞	ambient nanoparticle volume fraction
D_B	Brownian diffusion coefficient
D_T	thermophoretic diffusion coefficient
Ec	Eckert number
f	dimensionless stream function
g	gravitational acceleration
h	heat transfer coefficient
k	thermal conductivity of the base fluid
Le	Lewis number
M	Hartman number
N	concentration buoyancy
Nb	Brownian motion parameter
Nc	thermophoresis parameter
Nu_x	local Nusselt number
Pr	Prandtl number
q_m	wall mass flux
Q	heat generation/absorption
q_w	wall heat flux
R	Radiation parameter
Sh_x	local Sherwood number
T	nanofluid temperature
T_f	characteristic temperature
T_∞	ambient temperature of nanofluid
u	velocity component along x direction
u_w	stretching velocity of the sheet
v	velocity component along y direction
x	coordinate along the sheet
y	coordinate normal to the sheet
α	thermal diffusivity of base fluid
β	casson fluid parameter
β_c	concentration expansion coefficient
β_T	thermal expansion coefficient
η	similarity variable
μ	viscosity of the base fluid
ν	kinematic viscosity of the base fluid
λ	Mixed convection parameter
ϕ	dimensionless nanoparticle volume fraction
ψ	stream function
ρ	density of the base fluid
σ	thermal diffusivity
σ^*	electrical conductivity of the base fluid
σ_s	Stefan-Boltzmann constant
θ	dimensionless temperature
τ	ratio of specific heat capacities
τ_∞	surface shear stress
γ_1	Heat transfer Biot number
γ_2	Mass transfer Biot number
β_1	heat source/sink parameter
γ	Chemical reaction parameter